

On the cost of electro dialysis for the desalination of high salinity feeds

Ronan K. McGovern^a, Adam M. Weiner^a, Lige Sun^a, Chester G. Chambers^a, Syed M. Zubair^b,
John H. Lienhard V^a

^aCenter for Clean Water and Clean Energy, Massachusetts Institute of Technology, Cambridge, MA 02139, U.S.A.

^bKing Fahd University for Petroleum and Minerals, Dhahran, Saudi Arabia

Abstract

We propose the use of electro dialysis to desalinate produced waters from shale formations in order to facilitate water reuse in subsequent hydraulic fracturing processes. We focus on establishing the energy and equipment size required for the desalination of feed waters containing total dissolved solids of up to 192,000 ppm, and we do this by experimentally replicating the performance of a 10-stage electro dialysis system. We find that energy requirements are similar to current vapour compression desalination processes for feedwaters ranging between roughly 40,000-90,000 TDS, but we project water costs to potentially be lower. We also find that the cost per unit salt removed is significantly lower when removed from a high salinity stream as opposed to a low salinity stream, pointing towards the potential of ED to operate as a partial desalination process for high salinity waters. We then develop a numerical model for the system, validate it against experimental results and use this model to minimise salt removal costs by optimising the stack voltage. We find that the higher the salinity of the water from which salt is removed the smaller should be the ratio of the electrical current to its limiting value. We conclude, on the basis of energy and equipment costs, that electro dialysis processes are potentially feasible for the desalination of high salinity waters but require further investigation of robustness to fouling under field conditions.

Keywords: electro dialysis, desalination, brine concentration, energy efficiency, hydraulic fracturing, shale

1. Introduction

We have experimentally investigated factors affecting the cost of electro dialysis (ED) for the desalination of high salinity feeds, focusing on the dependence of the cost of salt removal upon dilute salinity. We have also developed a numerical model for the system, validated it against the experimental results and identified a strategy to optimise the stack voltage such that the sum of equipment and energy costs are minimised. Our motivation for this investigation was the desalination of produced waters in unconventional oil and gas extraction where, amongst other factors, the presence of high levels of total dissolved solids can disincentivise water reuse. Water reuse in hydraulic fracturing is of great interest both from an environmental perspective, as it reduces water use and minimises disposal through deep-well injection, but also from an economic perspective as water management costs can account for between 5 and 15% of drilling costs [1].

For the purpose of this investigation, we were most interested in flows of water during the life-cycle of a well, which are depicted in Fig. 1. For reuse to be economical, the savings in the sourcing, disposal and

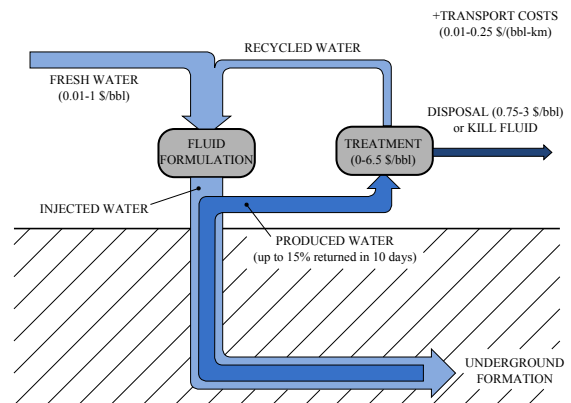


Figure 1: Fresh water [1] is mixed with recycled water and chemicals are added, that may include acids, friction reducers, gelling agents and proppant (sand) [2] to form the hydraulic fracturing fluid. The fluid is then injected into the well at high pressure to create fractures in the underlying shale formation. A portion of this fluid [3], perhaps in addition to fluid originally contained in the formations, subsequently returns to the surface, at a rate that generally decreases with time, and is known as produced water. The produced water may be: subjected to levels of treatment that vary from suspended solids removal to complete desalination [1] and recycling; sent to a disposal well; and/or employed elsewhere as a kill fluid (a fluid used to close off a well after production is complete) or as a salt based drilling fluid [1].

Email addresses: mcgov@alum.mit.edu (Ronan K. McGovern), lienhard@mit.edu (John H. Lienhard V)

24 transport of water must outweigh any increased costs 78
25 of treatment or of chemicals in the formulation of the 79
26 fracturing fluid. This means that regional differences 80
27 in recycling rates are strongly influenced by regional 81
28 differences in sourcing, disposal and transport costs. 82
29 For example, reuse rates are currently greatest in the 83
30 Marcellus shales [3] (reused water makes up 10-15% 84
31 of water needed to fracture a well) where transport and 85
32 disposal costs can reach \$15-18/bbl (\$94-113/m³) [4]. 86
33 The initial rate at which produced water flows to the 87
34 surface (e.g. within the first 10 days) also influences 88
35 the viability of reuse as low initial produced water vol- 89
36 ume flow rates making the logistics of reuse more dif- 90
37 ficult [3, 5]. 91

38 Moving to the costs of reuse, and setting aside the 92
39 expense associated with logistics, the costs come pri- 93
40 marily in the form of: increased water treatment costs; 94
41 increased chemical costs in the formulation of the hy- 95
42 draulic fracturing fluid to mitigate undesirable feed 96
43 water properties; and/or reduced oil or gas production 97
44 from the well. By and large, the increase in treatment 98
45 costs is highest, and the increase in chemical costs 99
46 lowest, when produced water is treated with mechani-100
47 cal vapour compression. Vapour compression provides101
48 high purity water for the formulation of the hydraulic102
49 fracturing fluid but is expensive. Ranges of roughly 5-103
50 8 kWh/bbl (32-50 kWh/m³) of distillate¹ [7] and 3.50-104
51 6.25 \$/bbl (\$22-39/m³) of distillate [1] have been re-105
52 ported for the treatment of produced waters. While106
53 vapour compression provides a high purity feed for107
54 the formulation of the hydraulic fracturing fluid, di-108
55 rect reuse, whereby produced water is directly blended109
56 with freshwater before formulation of the fracturing110
57 fluid, results, by and large, in the lowest treatment costs111
58 but greater chemical costs for fluid formulation and112
59 perhaps a decline in the well's production. Increased113
60 costs associated with reuse, depending on the degree114
61 of treatment employed, can come in the form of: in-115
62 creased friction reducer and scale inhibitor demand116
63 with high chloride contents; increased scaling within117
64 the shale formation with the presence of divalent ions;118
65 increased corrosion of pipes; increased levels of sul-119
66 phate reducing bacteria resulting in the production of120
67 H₂S gas [8]; and a reduction in the performance of121
68 coagulation/flocculation, flotation, gravity settling and122
69 plate and frame dewatering equipment due to residual123
70 unbroken polymer gel [9]. 124

71 Many of the challenges faced in reuse can be dealt125
72 with through primary treatment that removes sus-126
73 pended solids, oil, iron, unbroken polymers and bac-127
74 teria [9], generally at a cost much below complete de-128
75 salination (circa \$1/bbl (\$6.3/m³) compared to \$3.50-129
76 6.25/bbl (\$22-39/m³) for complete desalination [1]).130
77 The need for the removal of all solids, suspended131

¹6.4 kWh/bbl (40 kWh/m³) has been reported for 72.5% recovery133
of feedwater with total dissolved solids of 50,000 mg/L [6] 134

and dissolved, is less clear. Opinions vary as to the level of total dissolved solids (TDS) that can be tolerated [10] and a complete understanding of issues of chemical compatibility remains elusive [2]. There is evidence that, with improved chemical formulations, high salinity produced waters may be reused without desalination, particularly in the formulation of fluids for slickwater processes [11–16] (processes with high volume flow rates to avoid premature settling of sand, which serves to maintain fractures propped open) and to some extent for cross-linked gel fracturing processes [17] (lower volume flow rate processes employing low molecular weight guar gum based gels to ensure proppant remains suspended). However, the increase in chemical costs associated with such formulations not evident. Depending on the fracturing fluid desired, chemical use can be significant. Fedotov et al. [9] indicated that the use of drag reducing agents in slickwater fracturing processes, can reach approximately 1,000 ppm (2 lbs per 1,000 gallons), while for cross-linked gel fracturing processes chemical use can be much higher and reach 15,000 ppm (30 lbs/1,000 gallons).

In place of a distillation process, we propose the use of electrodialysis desalination to partially desalt produced water. The objective is to achieve a configuration that can reduce water treatment costs relative to distillation, by avoiding complete desalination, but can provide the benefit of reduced total dissolved solids relative to a direct reuse configuration. At present, a clear illustration of the dependence of ED salt removal costs on feed salinity is not present in literature, particularly for feed salinities above brackish. A number of studies consider seawater desalination with electrodialysis [18], including electrodialysis-reverse osmosis hybrid configurations [19], but focus upon energy costs alone. Lee et al. [20] consider the effect of feed salinity upon the cost of water from a continuous, as opposed to batch, electrodialysis system for brackish feed waters, McGovern et al. [21] analyse the dependence of water costs upon feed and product salinity in their analysis of hybrid ED-RO systems for brackish applications. Few studies exist that analyse both energy and capital costs for higher salinity feeds [22]. Batch studies of low salinity produced waters report energy consumption figures of 1.1 kWh/m³ for 90% TDS removal and 0.36 kWh/m³ for 50% TDS removal from a 3,000 ppm TDS stream [23]. A study at higher feed water salinity reports energy consumption of 12.4 kWh/m³ for 80,000 ppm TDS [24]. A number of experimental studies, with desalination occurring in a batch mode, report the process times required to achieve a final target purity as increasing with the feed salinity [25, 26] but leave unclear how process times translate into equipment costs. Furthermore, energy consumption in batch processes is often reported as an average kWh/kg salt removed for an entire pro-

cess without focusing on how this value varies depend-
ing upon the diluate, and to a lesser extent the concen-
trate, salinity.

In this work, we conduct multiple stages of batch
desalination on an experimental electro dialysis setup
such that each stage replicates closely a stage within a
continuous process. Furthermore, we relate batch pro-
cess times and energy consumptions to the production
rate and specific energy consumption that would be
achieved from an equivalent continuous system. Cou-
pled with a simple financial model, these metrics allow
us to investigate and optimise the dependence of cost
upon the feed salinity to a continuous electro dialysis
system.

2. Methods

2.1. Experimental

We performed an experiment to replicate the per-
formance of a ten stage continuous flow electro dial-
ysis system capable of desalinating a feed stream from
224 mS/cm (195,000 ppm TDS NaCl) down to 0.5
mS/cm (240 ppm TDS NaCl). We studied aqueous
NaCl solutions since Na^+ and Cl^- ions account for the
vast majority of dissolved solids contained within pro-
duced water samples taken from the Barnett, Eagle-
ford, Fayetteville, Haynesville, Marcellus and Bakken
shale plays [1]. Thus, the electrical conductivity and
chemical activity of salts in produced water samples
– both important influencers of the energy consump-
tion and system size in electro dialysis – are well sim-
ulated by aqueous NaCl solutions of matching total
dissolved solids. To do this, we ran ten batch exper-
iments, each representing a single stage in a continu-
ous process. We chose the diluate conductivities at the
start of each stage such that the diluate conductivity
was halved in each stage and the salt removal was ap-
proximately 50% per stage [20] (see Fig. 2). We chose
the concentrate concentration in each stage to replicate
the concentration that would prevail if the concentrate
salinity were to be determined solely by the rates of
salt and water transport across the membranes (see Ap-
pendix A.1). We held the stack voltage constant at 8 V
in all stages and chose this value such that the current
density at the end of the final stage would be 50% of
its limiting value (see Appendix A.2).

The experimental apparatus, illustrated in Fig. 3 in-
volved an ED200 stack [27] with 17 cell pairs consist-
ing of seventeen Neosepta AMS-SB, eighteen CMS-
SB membranes, thirty-four 0.5 mm spacers and two 1
mm end spacers. We employed a GW Instek GPR-
60600 and an Extech 382275 power supply to provide
current in the ranges of 0-5 A and 5-20 amps respec-
tively. We measured conductivity on a Jenco 3250
conductivity meter interfacing with model 106L (cell
constant, $K=1$) and model 107N (cell constant, $K=10$)

probes. We performed experiments in constant volt-
age mode, with current measured by an Extech EX542
multimeter. We determined initial diluate and concen-
trate volumes by summing the initial fluid volumes
contained within the beakers (1 litre and 3 litres for
the diluate and concentrate, respectively, in all tests)
with the internal volumes of the diluate and concen-
trate fluid circuits (see Appendix A.3). We determined
changes in diluate mass by tracking the mass of the
diluate within the beaker using an Ohaus Scout Pro
balance with a range of 0-2 kg. Changes in density
were also accounted for given knowledge of solution
conductivities versus time.

To quantify performance we considered certain key
performance metrics. The first metrics are specific pro-
cess times, based on stage salt removal, τ_i^s , and final
stage diluate volume, τ_i^w :

$$\tau_i^s = \frac{t_i}{(V_i^{in,d} C_i^{in,d} - V_i^{f,d} C_i^{f,d})} \quad (1)$$

$$\tau_i^w = \frac{t_i}{V_i^{f,d}} \quad (2)$$

where t_i is the process time for stage i , $V_i^{in,d}$ and $V_i^{f,d}$
are the initial and final stage volumes, and $C_i^{in,d}$ and
 $C_i^{f,d}$ are the initial and final stage concentrations. The
second metrics are specific energy consumption, based
on stage salt removal, E_i^s , and final stage diluate vol-
ume, E_i^w :

$$E_i^s = \frac{\sum_j I_{i,j} V_{i,j} \Delta t_{i,j}}{(V_i^{in,d} C_i^{in,d} - V_i^{f,d} C_i^{f,d})} \quad (3)$$

$$E_i^w = \frac{\sum_j I_{i,j} V_{i,j} \Delta t_{i,j}}{V_i^{f,d}} \quad (4)$$

where $I_{i,j}$ and $V_{i,j}$ are the stack current and voltage of
stage i in time period j of the process. $\Delta t_{i,j}$ refers to
time increment j of the process within stage i .

We used the above performance metrics to compute
cost metrics, employing the following simplifying as-
sumptions:

1. We set aside pre-treatment, post-treatment, main-
tenance and replacement costs, focusing solely
on the energy cost and upfront cost of electro-
dialysis equipment. These costs strongly de-
pend upon feedwater chemistry and can be sig-
nificant, *e.g.* the cost of basic pre-treatment for
waters produced from shale plays, which might
involve basic solids removal and/or COD and/or
BOD reduction, can fall in the region of \$1/bbl
(\$6.3/m³) [1].
2. We neglect pumping power costs (see Appendix
B for justification).
3. We assumed electricity to be priced at $K_E =$
\$0.15/kWh (a conservative estimate of gas pow-

Stage #	Stage 1	Stage 2	Stage 3	Stage 4	Stage 5	Stage 6	Stage 7	Stage 8	Stage 9	Stage 10
Concentrate	230 mS/cm (206,000 ppm)	200 mS/cm (162,000 ppm)	190 mS/cm (150,000 ppm)	180 mS/cm (139,000 ppm)	160 mS/cm (119,000 ppm)	150 mS/cm (109,000 ppm)	130 mS/cm (91,600 ppm)	100 mS/cm (67,200 ppm)	77 mS/cm (50,000 ppm)	52 mS/cm (33,000 ppm)
Initial Diluate	224 mS/cm (195,000 ppm)	192 mS/cm (152,000 ppm)	128 mS/cm (90,000 ppm)	64 mS/cm (40,700 ppm)	32 mS/cm (19,100 ppm)	16 mS/cm (9,010 ppm)	8 mS/cm (4,310 ppm)	4 mS/cm (2,070 ppm)	2 mS/cm (1,010 ppm)	1 mS/cm (492 ppm)
Final Diluate	192 mS/cm (152,000 ppm)	128 mS/cm (90,000 ppm)	64 mS/cm (40,700 ppm)	32 mS/cm (19,100 ppm)	16 mS/cm (9,010 ppm)	8 mS/cm (4,310 ppm)	4 mS/cm (2,070 ppm)	2 mS/cm (1,010 ppm)	1 mS/cm (492 ppm)	0.5 mS/cm (242 ppm)

Figure 2: We designed each of the ten stages such that the diluate conductivity was halved in each successive stage, with the exception of the first two stages. We reduced the salt removal in the first two stages to avoid the depletion of water in the diluate beaker before the end of a trial. We chose concentrate conductivities based on the rates of salt and water transport across the membranes (see Appendix A.1).

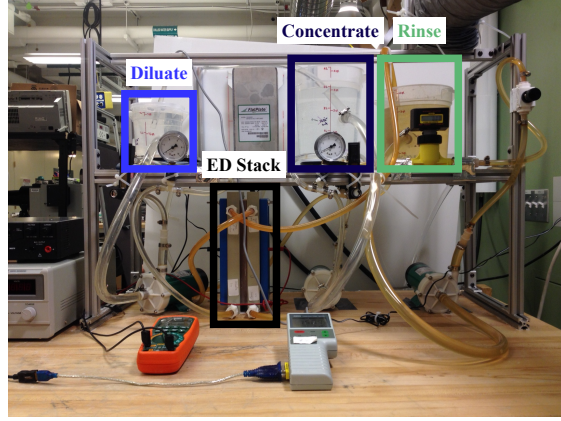
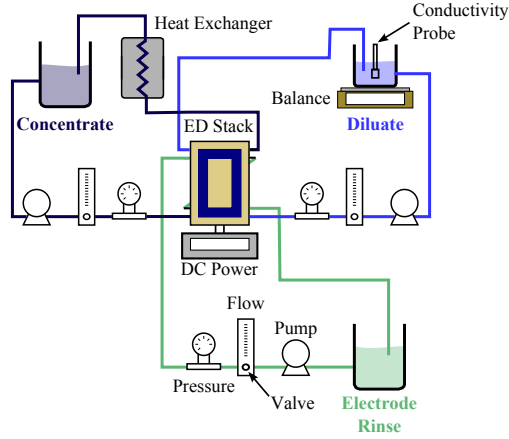


Figure 3: The electrodesialysis setup consisted of a diluate, concentrate, and rinse circuit feeding an ED200 stack. We employed a heat exchanger to regulate the temperature of the concentrate, with the stack effectively operating as a second heat exchanger to regulate the diluate temperature. We employed valved-rotameters to regulate the flow rates in each circuit.

ered distributed generation [28]).

- We assumed equipment costs to scale with membrane area and computed these costs by considering an equipment cost per unit membrane area of $K_Q = 1500$ \$/m² (based upon the capital cost data collected by Sajtar and Bagley [29] and analysed by McGovern et al. [21]). This cost data covers plant sizes up to 40000 m³ per day and feed salinities up to 7,000 mg/L. Its extrapolation to higher salinities is based on the assumption that similar stack designs would be employed at both high and low salinity.
- We assumed the total installed cost of the equipment to equal three times the estimated equipment costs [30]. This is an estimate since no data exists on commercial scale electrodesialysis installations in shale plays.
- We amortised equipment costs over a twenty-year life, $T = 20$ years, assuming an annualised cost of capital of $r = 10\%$.

Given these assumptions, we defined the specific cost of salt removal, in \$/lb salt (or \$/kg salt) and the specific cost of product water \$/bbl (or \$/m³) from

each stage:

$$\Xi_i^s = K_E E_i^s + \frac{K_Q A_m}{\frac{1}{r} \left[1 - \left(\frac{1}{1+r} \right)^T \right]} \tau_i^s \quad (5)$$

$$\Xi_i^w = K_E E_i^w + \frac{K_Q A_m}{\frac{1}{r} \left[1 - \left(\frac{1}{1+r} \right)^T \right]} \tau_i^w \quad (6)$$

where A_m is the total membrane area in the stack.

2.2. Model

To minimise the cost of salt removal, through optimisation of the stack voltage, we constructed a semi-empirical model for the electrodesialysis system, which we validated with experimental results. The process time, energy consumption, and cost of salt removal from each stage were computed using a numerical model that broke each stage into twenty time periods, with an equal change in diluate salinity in each period. During each of these periods the stack voltage and rates of salt and water transport were approximated as constant and used, in conjunction with molar conservation equations, to determine the conditions at the start of the next period. Within each stage, the number of moles of salt and water present in the diluate at the start and the end of each time step j are related to the molar fluxes

of salt and water, $J_{s,j}$ and $J_{w,j}$ and the total cell pair area, A_m :

$$N_{s,j+1} - N_{s,j} = -A_m J_{s,j} \quad (7)$$

$$N_{w,j+1} - N_{w,j} = -A_m J_{w,j} \quad (8)$$

with N_{j+1} and N_j the number of moles of salt, s , or water, w , at the end or start of each time step, A_m the total cell pair area of the stack and J_j the average flux across the membrane area of salt, s , or water, w , at time step j . The concentrate conductivity was approximated as constant in time for each stage and equal to the value employed in experiments. At each instant in time the diluate concentration is approximated as uniform across the membrane area. This is because the time taken for fluid to travel the length of the membrane (<8 s) is much less than the stage processing time (>120 s for all stages).

Salt, water, and charge transport were modelled based upon the approach taken in previous work [31, 32]. Salt transport was modelled by a combination of migration and diffusion:

$$J_s = N_{cp} \left[\frac{T_s^{cp} i}{F} - L_s (C_{s,c,m} - C_{s,d,m}) \right] \quad (9)$$

and water transport by a combination of migration (electro-osmosis) and osmosis:

$$J_w = N_{cp} \left[\frac{T_w^{cp} i}{F} - L_w (\pi_{s,c,m} - \pi_{s,d,m}) \right]. \quad (10)$$

In Eq. (10), N_{cp} is the number of cell pairs, T_s^{cp} and T_w^{cp} are the overall salt and water transport numbers for the cell pair, L_s and L_w are the overall salt and water permeabilities of the cell pair, C denotes concentration in moles per unit volume, and π denotes osmotic pressure (calculated employing osmotic coefficients for aqueous NaCl from Robinson and Stokes [33]). The difference between membrane surface concentrations, $C_{s,c,m}$ and $C_{s,d,m}$, and bulk concentrations, $C_{s,c}$ and $C_{s,d}$, was computed via a convection-diffusion based model for concentration polarisation (see Appendix C.1).

The stack voltage was represented as the sum of ohmic terms and membrane potentials:

$$V_{stack} = N_{cp} \left(\bar{r}_{am} + \bar{r}_{cm} + \frac{h_d}{\sigma \Lambda_d C_d} + \frac{h_c}{\sigma \Lambda_c C_c} \right) i + \bar{r}_{cm} i + \frac{2h_r}{\sigma k_r} i + N_{cp} (E_{am} + E_{cm}) + V_{el} \quad (11)$$

where Λ is the molar conductivity, itself taken to be a function of concentration [34, 35] and h denotes channel height. k denotes electrical conductivity, the subscript r denotes the rinse solution, σ denotes the spacer shadow factor, \bar{r} denotes the membrane surface resistance of the anion or cation exchange membrane and V_{el} denotes the sum of the anode and cathode electrode

potentials. Junction potentials associated with concentration differences across boundary layers were neglected while membrane potentials E_{am} and E_{cm} were computed assuming quasi-equilibrium salt and water migration through the membranes (see Appendix C.2).

A series of calibration tests was conducted to establish the values of T_s^{cp} , T_w^{cp} , L_s , L_w , r_m , σ , V_{el} and the Sherwood number Sh (see Appendix D). Each test was repeated three times to ensure repeatability. Bias errors arising from the determination of the diluate circuit volume (Appendix A.3) and of leakage rates from diluate to concentrate were propagated through the equations defining these nine parameters and combined with the random error [Eq. (12)] that was determined from the sample standard deviation of results computed from the three tests. Errors are computed at a 68% confidence level.

$$\epsilon_{tot}^2 = \epsilon_{bias}^2 + \epsilon_{random}^2 \quad (12)$$

Salt and water transport numbers, T_s^{cp} and T_w^{cp} , were determined via constant current migration tests where the diluate and concentrate conductivities were close to one another. Salt and water permeabilities, L_s and L_w , were determined via diffusion tests with zero current and initial diluate concentrations close to zero. Membrane resistance, r_m , the spacer shadow factor, σ , the electrode potential, V_{el} , and the Sherwood number, Sh , were determined from voltage-current tests at constant diluate and concentrate salinity.

3. Results: Process time, energy consumption and costs

The process time, energy and cost requirements of electro dialysis treatment are shown on a unit salt removal basis in Figs. 4, 5 and 6 and on a unit product water basis in Figs. 7, 8 and 9, in each case illustrating agreement, within error, between the model and the experiment. The deviation between the model and experiment is greatest in the final stages, where the modelled values of energy consumption and process time are highly sensitive to the electrode potential. This is because the driving force for salt transport is the difference between the stack voltage and the sum of the electrode potentials and membrane potentials ($V^{stack} - N_{cp} (E_{am} + E_{cm}) - V_{el}$). The sum of membrane potentials, $E_{am} + E_{cm}$, scales with the natural logarithm of the salinity ratio (concentrate to diluate) [32] and therefore, in the final stage where the diluate salinity is lowest, the sum of the membrane potentials is greatest — accounting for over 50% of the 8 V applied across the stack. This remaining voltage driving salt transport is therefore highly sensitive to the modelled value of the electrode potential ($V_{el}=2.13 \pm 0.3$ V). This sensitivity further posed a difficulty in modelling desalination, within the final stage, down to 0.5 mS/cm (242 ppm

314 TDS). The modelled value of the electrode potential (in
 315 combination with the modelled values of other fitted
 316 parameters, see Appendix D) was such that the back
 317 diffusion of salt outweighed salt removal via migration
 318 before a conductivity of 0.5 mS/cm was reached. For
 319 this reason, the model of the final stage is for an fi-
 320 nal diluate conductivity of 0.55 mS/cm rather than 0.5
 321 mS/cm.

The trends in process time, energy and cost are most easily explained by considering these quantities on the basis of salt removal. Here we provide scaling estimates that describe the first order variation in process time, energy and cost with stage number. The process time τ for any given stage scales with the change in salinity in that stage ΔS and the inverse of the current I , which describes the number of moles of salt removed per coulomb of charge:

$$\tau \sim \frac{\Delta S}{I} \quad (13)$$

Meanwhile, the current scales approximately with the quotient of the stack voltage over the stack resistance:

$$I \sim \frac{V_{st}}{R_{st}}. \quad (14)$$

The stack resistance scales with the sum of the mem-
 brane, concentrate and diluate resistances:

$$R_{st} \sim \left(2r_m + \frac{h}{\sigma k_c} + \frac{h}{\sigma k_d} \right) \quad (15)$$

where σ is the spacer shadow factor, h is the diluate and concentrate channel height, k is the solution conductivity of the diluate d or the concentrate c , and r_m is the anion or cation exchange membrane surface resistance. The process time therefore scales approximately as:

$$\tau \sim \frac{\Delta S}{V} \left(2r_m + \frac{h}{\sigma k_c} + \frac{h}{\sigma k_d} \right). \quad (16)$$

322 At high diluate conductivity (lower number stages in
 323 Fig. 2) the membrane resistance dominates the stack
 324 resistance and thus the diluate and concentrate conduc-
 325 tivities have a weak effect on process time. At low dilu-
 326 ate conductivity (high number stages) the diluate resis-
 327 tance dominates the stack resistance and the process
 328 time per unit salt removed scales roughly with the in-
 329 verse of the diluate conductivity. The stack resistance
 330 roughly doubles in moving from one stage to the next
 331 and so too does the specific process time.

The energy consumption per unit salt removed, E^s , for any given stage scales with the product of voltage, the current and the process time divided by the change

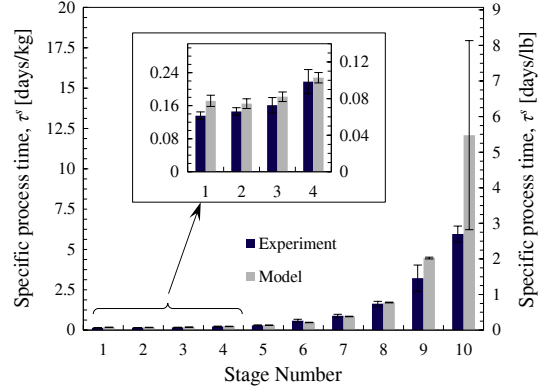


Figure 4: Stage process time per unit of salt removed.

in salinity:

$$E^s \sim \frac{VI\tau^s}{\Delta S}. \quad (17)$$

Considering how process time scales in Eq. (13) it is clear that the energy consumption per unit salt removed scales with the quotient of the voltage over the salt transport number:

$$E^s \sim V. \quad (18)$$

Thus, while process time varies significantly with stage number (note the \log_2 scale in Fig. 4) specific energy consumption (plotted on a linear scale in Fig. 5) remains relatively constant.

Given the above explanations for the trends in process time and energy, on the basis of unit salt removal, it is clear that the cost per unit of salt removal must remain relatively constant at low stage numbers (high diluate salinities) but will rise rapidly due to increasing equipment costs at higher number stages (lower salinities) as seen in Fig. 6.

Combining these insights on Fig. 4, 5 and 6 with the fact that salt removal is approximately halved in each stage moving from stage 3 to stage 10 we can easily explain the trends on a basis of stage product water, seen in Fig. 7, 8 and 9. Specific process time on the basis of water produced falls with an increasing stage number because the processing time per unit of salt removed (Fig. 4) rises more slowly than the quantity of salt removed per stage (see Fig. 2). Specific energy consumption, on the basis of product water, falls because energy consumption per unit of salt removed is approximately constant (see Fig. 4) and the quantity of salt removed per stage falls rapidly (see Fig. 2). As a consequence of falling τ^w and E^w with increasing stage number, the specific cost of water also falls in moving to higher stage numbers, primarily because the quantity of salt removed per stage is falling rapidly.

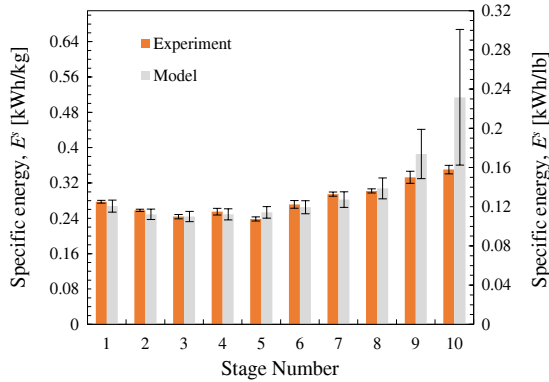


Figure 5: Stage energy consumption per unit of salt removed.

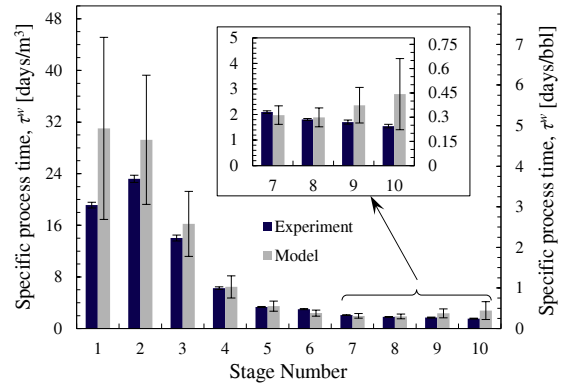


Figure 7: Stage process time per unit of product water.

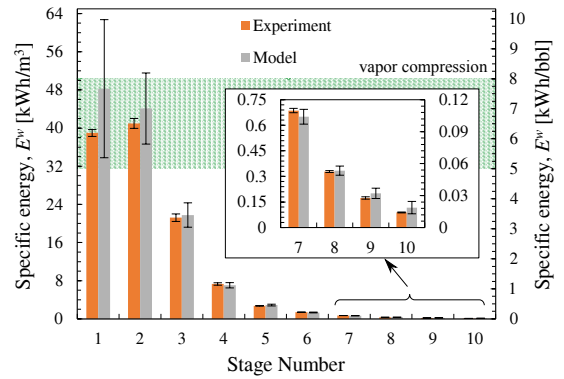


Figure 8: Stage energy per unit of product water. The range of energy consumption for vapour compression is taken from Hayes and Severin for 72.5% recovery of feedwater with TDS of 50,000 mg/L (corresponding roughly to stages 4 through 10) [6].

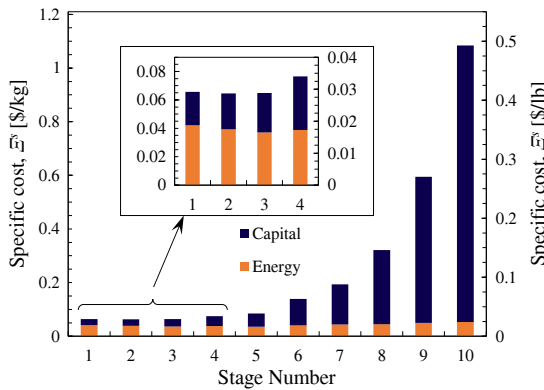


Figure 6: Stage cost per unit of salt removed (based on experimental results).

3.1. Discussion

Not included in the computation of energy in Fig. 5 or Fig. 8 is energy required for pumping, shown in Fig. 10. These values for pumping power are computed via experimental measurements of the pressure drop across the stack and assuming 100% pump efficiency (see Appendix B for detailed calculations). Comparing these values to those for stack energy consumption in Fig. 8, it is clear that pumping power accounts for a significant portion of total power consumption only at low diluate salinity (e.g. stages 10, 9 and 8 where salt removal rates are lowest). Importantly, these values of pumping power for a laboratory scale system are unlikely to be representative of pumping power consumption in a large scale system. This is because the processing length of the system investigated is only 20 cm, meaning that entrance and exit head loss has a disproportionately large effect on the pumping power relative to frictional pressure drop within the membranes, which would be expected to dominate in large scale systems with larger processing lengths.

The range of energy requirements for vapour compression shown in Fig. 8, and of water costs shown in Fig. 9, correspond roughly to a feed salinity equal

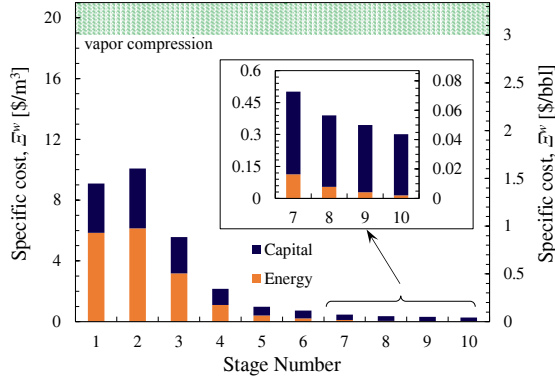


Figure 9: Stage cost per unit of product water (based on experimental results). The range of water costs for vapour compression is taken from Slutz et al., wherein cases are considered with feedwater TDS of 49,500 and 80,000 mg/L (corresponding roughly to stages through 10 and 3 through 10, respectively) [1].

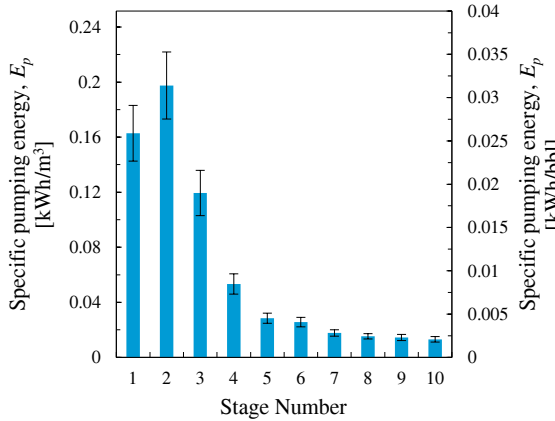


Figure 10: Energy consumption associated with pumping power.

to that of the 3rd or 4th stages of electro dialysis. On this basis, Figs. 8 and 9 indicate that electro dialysis can achieve almost complete salt removal with similar energy requirements and lower water costs than vapour compression [1, 6]. Furthermore, considering electro dialysis costs on the basis of salt removal (Fig. 6), it is interesting that costs fall significantly at higher salinity (e.g. in lower number stages). This points to the potential of electro dialysis for the partial desalination of high salinity feed streams.

For electro dialysis systems to be realised for high salinity produced waters, further work is required to address the risks of scaling and fouling. Future work will need to go beyond the simplified solution chemistries considered to date [25, 26], and in this work. Produced waters from shale plays have been shown to contain significant concentrations of dissolved solids with low solubility, including silica, iron, barium and calcium [1, 36]. Furthermore, produced waters may contain significant levels of total organic carbons (up to 160 mg/L, depending on the method used for oil-water separation [37]), while ED manufacturers advise against feedwater total organic carbon concentrations above 15 mg/L [38] and a number of studies reveal difficulties in removing total organic carbon with traditional filtration methods [39, 40].

4. Voltage optimisation

Having validated a numerical model for the system we optimise the voltage in each stage to minimise the costs of salt removal. In Fig. 11, we compare three distinct strategies that are shown in Fig. 12:

1. a constant voltage strategy where the voltage is set such that the current density is 80% of its limiting value at the end of stage 10 ($V_{stack,i} = 16$ V, see Fig. A.1);
2. a constant voltage strategy where the voltage is set such that the current density is 50% of its limiting value at the end of stage 10 ($V_{stack,i} = 8$ V, see Fig. A.1); and
3. an optimised strategy where the total costs per stage (equipment and energy) are numerically minimised using a quadratic method [41] to identify an optimal voltage $V_{stack,i}^*$.

Figure 11 reveals that in higher number stages (lower diluate salinities) the strategy of setting the voltage such that the current is just below its limiting value (e.g., 80%) is a good one as this greatly reduces equipment costs. However, at higher salinities (lower stage numbers), it is best to operate with a lower stack voltage that allows for reduced energy consumption. Of course, depending on the relative price of equipment to energy the optimal stack voltage for each stage will differ. Higher electricity prices will drive lower optimal stack voltages and vice-versa. Nevertheless, it is

438 clear that the brackish water strategy of setting the cur-480
439 rent close to its limiting value [20] is not necessarily
440 optimal for the treatment of higher salinity waters. 481

441 5. Conclusions 482

442 Our experimental and economic assessment of elec-485
443 trodialysis at salinities up to 192,000 ppm NaCl in-486
444 dicates good potential for the process at high salini-487
445 ties, such as those seen in produced waters from hy-488
446 draulically fractured shales. For feedwaters with TDS
447 of roughly 40,000-90,000 ppm, we show that energy 489
448 requirements are similar and project that combined
449 equipment and energy costs are potentially lower for 490
450 electro dialysis relative to vapour compression. If par-491
451 tial, as opposed to complete, desalination of a feed wa-492
452 ter is required, the prospects for ED are even greater, 493
453 as the cost per unit of salt removed is much lower at 494
454 high diluate salinities. For example, salt removal from 495
455 a stream of 500 ppm TDS might cost up to four times 496
456 that of salt removal from a stream at 192,000 ppm TDS, 497
457 per unit of salt removed. 500

458 Beyond our experimental assessment of electro dial-501
459 ysis at high salinities, we have developed and validated 502
460 a numerical model covering a range of diluate salin-503
461 ities from 250 ppm up to 192,000 ppm NaCl. This 504
462 model reveals the importance of optimising the stack 505
463 voltage to minimise salt removal costs. For the set of 506
464 equipment and energy prices examined, we found that 507
465 brackish water desalination costs are minimised by op-508
466 erating close to the limiting current density, while for 509
467 salt removal from higher salinity streams lower stack 510
468 voltages can allow cost reductions of up to 30%. 511

469 This analysis addresses two major considerations 515
470 affecting the viability of ED for the desalination of 516
471 high salinity produced waters, namely the energy and 517
472 equipment requirements. Given that ED compares 518
473 favourably with vapour compression on these metrics, 519
474 a more detailed analysis of an ED system under field 520
475 conditions is warranted. This might include studies of 521
476 system fouling and scaling when treating more com-522
477 plex feed waters and an analysis of feedwater pre-523
478 treatment requirements and costs to ensure robust op-524
479 eration. 525

6. Acknowledgements 482

The authors acknowledge support from the King Fahd University of Petroleum and Minerals through the Center for Clean Water and Clean Energy at MIT and KFUPM under project number R15-CW-11. Ronan McGovern and Chester Chambers acknowledge support from the Hugh Hampton Young Memorial Fellowship and partial UROP support from the MIT Energy Initiative, respectively.

7. References 482

- [1] J. A. Slutz, J. A. Anderson, R. Broderick, P. H. Horner, et al., Key shale gas water management strategies: An economic assessment, in: International Conference on Health Safety and Environment in Oil and Gas Exploration and Production, Society of Petroleum Engineers, 2012.
- [2] R. Vidic, S. Brantley, J. Vandenbossche, D. Yoxtheimer, J. Abad, Impact of shale gas development on regional water quality, *Science* 340 (6134).
- [3] M. E. Mantell, Produced water reuse and recycling challenges and opportunities across major shale plays, in: Proceedings of the Technical Workshops for the Hydraulic Fracturing Study: Water Resources Management. EPA, Vol. 600, 2011, pp. 49–57.
- [4] S. Shipman, D. McConnell, M. P. Mccutchan, K. Seth, et al., Maximizing flowback reuse and reducing freshwater demand: Case studies from the challenging marcellus shale, in: SPE Eastern Regional Meeting, Society of Petroleum Engineers, 2013.
- [5] J.-P. Nicot, B. R. Scanlon, R. C. Reedy, R. A. Costley, Source and fate of hydraulic fracturing water in the barnett shale: A historical perspective, *Environmental science & technology*.
- [6] T. Hayes, B. F. Severin, P. S. P. Engineer, M. Okemos, Barnett and appalachian shale water management and reuse technologies, *Contract 8122 (2012) 05*.
- [7] P. Horner, J. A. Slutz, Shale gas water treatment value chain - a review of technologies, including case studies, in: SPE Annual Technical Conference and Exhibition, no. SPE 147264, Society of Petroleum Engineers, 2011.
- [8] Proceedings and Minutes of the Hydraulic Fracturing Expert Panel XTO Facilities, Fort Worth September 26th, 2007.
- [9] V. Fedotov, D. Gallo, P. M. Hagemeyer, C. Kuijvenhoven, et al., Water management approach for shale operations in north america, in: SPE Unconventional Resources Conference and Exhibition-Asia Pacific, Society of Petroleum Engineers, 2013.
- [10] S. Rassenfoss, From flowback to fracturing: water recycling grows in the marcellus shale, *Journal of Petroleum Technology* 63 (7) (2011) 48–51.
- [11] J. Bryant, I. Robb, T. Welton, J. Haggstrom, Maximizing friction reduction performance using flow back water and produced water for waterfrac applications, in: AIPG Marcellus Shale Hydraulic Fracturing Conference, 2010.
- [12] A. Kamel, S. N. Shah, Effects of salinity and temperature on drag reduction characteristics of polymers in straight circular pipes, *Journal of petroleum Science and Engineering* 67 (1) (2009) 23–33.
- [13] J. Paktinat, O. Bill, M. Tulissi, Case studies: Improved performance of high brine friction reducers in fracturing shale reservoirs, *Society of Petroleum Engineers* (2011) 1–12.
- [14] C. W. Aften, Study of friction reducers for recycled stimulation fluids in environmentally sensitive regions, in: SPE Eastern Regional Meeting, Society of Petroleum Engineers, 2010.
- [15] M. J. Zhou, M. Baltazar, Q. Qu, H. Sun, Water-based environmentally preferred friction reducer in ultrahigh-tds produced water for slickwater fracturing in shale reservoirs, in:

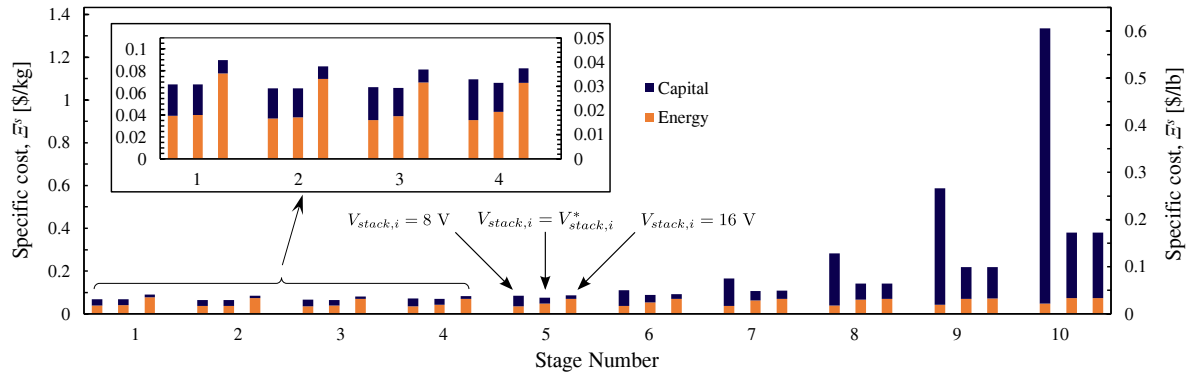


Figure 11: Effect of voltage strategy upon the cost of salt removal.

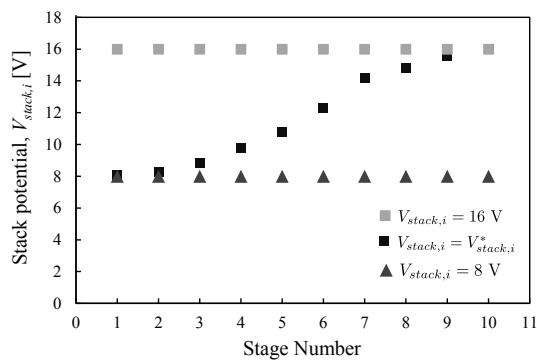


Figure 12: Effect of voltage strategy upon the optimal voltage. At low stage numbers the $V_{stack,i} = 8$ V strategy is close to optimal while at high stage numbers the $V_{stack,i} = 16$ V is closest to optimal.

545 SPE/EAGE European Unconventional Resources Conference
 546 and Exhibition, Society of Petroleum Engineers, 2014.
 547 [16] J. K. Hallock, R. L. Roell, P. B. Eichelberger, X. V. Qiu, C. C.
 548 Anderson, M. L. Ferguson, Innovative friction reducer pro-
 549 vides improved performance and greater flexibility in recycling
 550 highly mineralized produced brines, in: SPE Unconventional
 551 Resources Conference-USA, Society of Petroleum Engineers,
 552 2013.
 553 [17] R. LeBas, P. Lord, D. Luna, T. Shahan, Development and use
 554 of high-tds recycled produced water for crosslinked-gel-based
 555 hydraulic fracturing, in: 2013 SPE Hydraulic Fracturing Tech-
 556 nology Conference, 2013.
 557 [18] M. Turek, Dual-purpose desalination-salt production electro-
 558 dialysis, *Desalination* 153 (1) (2003) 377–381.
 559 [19] A. Galama, M. Saakes, H. Bruning, H. Rijnaarts, J. Post, Sea-
 560 water pre-desalination with electro-dialysis, *Desalination* 342
 561 (2013) 61–69.
 562 [20] H.-J. Lee, F. Sarfert, H. Strathmann, S.-H. Moon, Designing
 563 of an electro-dialysis desalination plant, *Desalination* 142 (3)
 564 (2002) 267–286.
 565 [21] R. K. McGovern, S. M. Zubair, J. H. Lienhard V, The benefits
 566 of hybridising electro-dialysis with reverse osmosis, *Journal of*
 567 *Membrane Science* 469 (2014) 326 – 335.
 568 [22] R. K. McGovern, S. M. Zubair, J. H. Lienhard V, Hybrid elec-
 569 tro-dialysis reverse osmosis system design and its optimization
 570 for treatment of highly saline brines, *IDA Journal of Desalina-
 571 tion and Water Reuse* 6 (1) (2014) 15–23.
 572 [23] T. Brown, C. D. Frost, T. D. Hayes, L. A. Heath, D. W. John-
 573 son, D. A. Lopez, D. Saffer, M. A. Urynowicz, J. Wheaton,

574 M. D. Zoback, Produced water management and beneficial
 575 use, Tech. rep., DOE Award No.: DE-FC26-05NT15549
 576 (2009).
 577 [24] M. Turek, Electro-dialytic desalination and concentration of
 578 coal-mine brine, *Desalination* 162 (2004) 355–359.
 579 [25] L. Dallbauman, T. Sirivedhin, Reclamation of produced water
 580 for beneficial use, *Separation science and technology* 40 (1-3)
 581 (2005) 185–200.
 582 [26] T. Sirivedhin, J. McCue, L. Dallbauman, Reclaiming produced
 583 water for beneficial use: salt removal by electro-dialysis, *Journal of membrane science* 243 (1) (2004) 335–343.
 584 [27] PCCell GmbH, ED 200, Lebacher Strasse 60, D-66265
 585 Heusweiler, Germany.
 586 URL <http://www.pca-gmbh.com/pccel1/ed200.htm>
 587 [28] R. F. Stiles, M. S. Slezak, Strategies for reducing oilfield elec-
 588 tric power costs in a deregulated market, *SPE production &*
 589 *facilities* 17 (03) (2002) 171–178.
 590 [29] E. T. Sajtar, D. M. Bagley, Electro-dialysis reversal: Process
 591 and cost approximations for treating coal-bed methane waters,
 592 *Desalination and Water Treatment* 2 (1-3) (2009) 284–294.
 593 [30] M. S. Peters, K. D. Timmerhaus, R. E. West, K. Timmerhaus,
 594 R. West, *Plant design and economics for chemical engineers*,
 595 Vol. 4, McGraw-Hill New York, 1968.
 596 [31] M. Fidaleo, M. Moresi, Optimal strategy to model the electro-
 597 dialytic recovery of a strong electrolyte, *Journal of Membrane*
 598 *Science* 260 (1) (2005) 90–111.
 599 [32] R. K. McGovern, S. M. Zubair, J. H. Lienhard V, The cost ef-
 600 fectiveness of electro-dialysis for diverse salinity applications,
 601 *Desalination* 348 (2014) 57–65.
 602 [33] R. Robinson, R. Stokes, *Electrolyte Solutions*, Courier Dover
 603 Publications, 2002.
 604 [34] T. Shedlovsky, The electrolytic conductivity of some uni-
 605 valent electrolytes in water at 25 C, *Journal of the American*
 606 *Chemical Society* 54 (4) (1932) 1411–1428.
 607 [35] J. Chambers, J. M. Stokes, R. Stokes, Conductances of concen-
 608 trated aqueous sodium and potassium chloride solutions at 25
 609 C, *The Journal of Physical Chemistry* 60 (7) (1956) 985–986.
 610 [36] G. P. Thiel, J. H. Lienhard V, Treating produced water from hy-
 611 draulic fracturing: Composition effects on scale formation and
 612 desalination system selection, *Desalination* 346 (2014) 54–69.
 613 [37] J. M. Silva, Produced water pretreatment for water recovery
 614 and salt production, Tech. rep., Research Partnership to Secure
 615 Energy for America (2012).
 616 [38] GE Power & Water, GE 2020 EDR Systems (2013).
 617 [39] Q. Jiang, J. Rentschler, R. Perrone, K. Liu, Application of ce-
 618 ramic membrane and ion-exchange for the treatment of the
 619 flowback water from marcellus shale gas production, *Journal of*
 620 *Membrane Science* 431 (2013) 55–61.
 621 [40] M. M. Michel, L. Reczek, Pre-treatment of flowback water to
 622 desalination, *Monographs of the Environmental Engineering*
 623 *Committee* 119 (2014) 309–321.

625	[41] S. A. Klein, Engineering Equation Solver, Academic Profes-	683	V_{corr}	stack voltage corrected for concentration	
626	sional V9.438-3D (2013).	684		polarisation, V	
627	[42] M. Fidaleo, M. Moresi, Electrodialytic desalting of model con-	685	V_{stack}	stack voltage, V	
628	centrated nacl brines as such or enriched with a non-electrolyte	686	V	volume, m ³	
629	osmotic component, Journal of Membrane Science 367 (1)	687	\dot{V}	volume flow rate, m ³ /s	
630	(2011) 220–232.	688	w	mass, lbs or kg	
631	[43] A. Sonin, R. Probstein, A hydrodynamic theory of desalination,	689	x	concentration, mol salt/mol water	
632	by electrodialysis, Desalination 5 (3) (1968) 293–329.				
633	[44] O. Kuroda, S. Takahashi, M. Nomura, Characteristics of flow				
634	and mass transfer rate in an electrodialyzer compartment in-				
635	cluding spacer, Desalination 46 (1) (1983) 225–232.	690	<i>Greek Symbols</i>		
636	[45] E. R. Association, Viscosity of Water and Steam, Edward	691	Δ	change	
637	Arnold Publishers, 1967.	692	ϵ	error	
638	[46] ASTM Corporation, Neosepta, URL: http://www.astom-	693	Λ	molar conductivity, S m ² /mol	
639	corp.jp/en/en-main2-neosepta.html (2013).	694	μ	chemical potential, J/mol	
640	[47] K. Kontturi, L. Murtomaki, J. A. Manzanares, Ionic Transport	695	ν	viscosity, m ² /s	
641	Processes In Electrochemistry and Membrane Science, Ox-	696	Ξ^s	specific cost of salt, \$/lb or \$/kg	
642	ford, 2008.	697	Ξ^w	specific cost of water, \$/bbl or \$/m ³	
643	[48] N. Berezina, N. Gnsin, O. Dyomina, S. Timofeyev, Water	698	π	osmotic pressure, bar	
644	electrotransport in membrane systems. experiment and model	699	ρ	density, kg/m ³	
645	description, Journal of membrane science 86 (3) (1994) 207–	700	σ	spacer shadow factor, -	
646	229.	701	τ^s	specific process time, days/lb or days/kg	
		702	τ^w	specific process time, days/bbl or	
		703		days/m ³	
647	Nomenclature				
648	<i>Roman Symbols</i>				
649	A_m	membrane area, m ²	704	<i>Subscripts</i>	
650	C	concentration, mol/m ³	705	am	anion exchange membrane
651	D	diffusivity, m ² /s	706	c	concentrate
652	E^s	specific energy of salt removal, kWh/lb	707	$circ$	circuit
653		or kWh/kg	708	cm	cation exchange membrane
654	E^w	specific energy of water produced,	709	d	diluate
655		kWh/bbl or kWh/m ³	710	el	electrode
656	h	channel height, m	711	i	stage number
657	i	current density, A/m ²	712	j	time period
658	I	current, A	713	m	membrane surface
659	k	conductivity, S/m	714	p	pump
660	K_E	energy price, \$/kWh	715	r	rinse
661	K_Q	area normalised equipment price, \$/m ²	716	s	salt
662		membrane	717	s	water
663	L_s	membrane salt permeability, m ² /s			
664	L_w	membrane water permeability,	718	<i>Superscripts</i>	
665		mol/m ² s bar	719	f	final
666	m	slope	720	in	initial
667	M	molar mass, kg/mol			
668	m_s	molal concentration, mol/kg w			
669	N	number of moles, mol			
670	n_{cp}	number of cell pairs, -			
671	\bar{r}	membrane surface resistance, Ω m ²			
672	R	universal gas constant, J/mol K			
673	Re	Reynolds number			
674	Sc	Schmidt number			
675	Sh	Sherwood number			
676	t	process time, s			
677	T	system life, years			
678	\bar{T}_{cu}	integral membrane counterion transport			
679		number, -			
680	t_{cu}	solution counter-ion transport number, -			
681	T_s^{cp}	cell pair salt transport number, -			
682	T_w^{cp}	cell pair water transport number, -			

721 **Appendix A. Determination of experimental conditions**
722

723 *Appendix A.1. Determination of the concentrate salinity in each stage*
724

A key benefit of multi-staging the ED process at high salinities is the possibility of selecting a different concentrate salinity in each stage. If the concentrate salinity were to be the same in all stages it would necessarily be greater than the diluate salinity in the first stage. This would result in very strong salt diffusion from concentrate to diluate and water osmosis from diluate to concentrate in the final stages where the diluate salinity would be much lower than the concentrate. In our experiment we therefore choose higher concentrate salinities in stages with higher diluate salinities and vice versa. In each stage we set the concentrate salinity equal to the steady state salinity that would be dictated by the relative rates of salt and water transport across the membranes:

$$x_{s,c} = \frac{J_s}{J_s + J_w} \quad (\text{A.1})$$

725 where $x_{s,c}$ is the mole fraction of salt in the concentrate
726 at steady state. To compute each steady-state concentra-
727 tate value we modelled salt and water transport using
728 the methods of Section 4. Rather than modelling the 756
729 steady state concentrate salinity for each stage we 757
730 approximated its value by considering the molar fluxes of
731 salt and water at the very end of each stage.

732 Since the fitted parameters required for the model
733 were not known a priori, we considered values from
734 the literature for similar ED experiments (Table A.1).
735 Furthermore, in practice an ED system operator may
736 choose to run the stacks with a lower concentrate salin-
737 ity than could be reached in steady state, perhaps to
738 avoid scale formation. The concentrate salinities chosen
739 for a given application may not exactly match the
740 present study. Nonetheless, the results obtained remain
741 significant as stack performance is primarily affected
742 by the diluate conductivity and membrane resistance
743 rather than concentrate salinity, as explained in Sec-
744 tion 3.

745 *Appendix A.2. Selection of the stack voltage*

746 We selected a constant operating voltage of 8 V,
747 which ensured that we never exceeded 50% of the lim-
748 iting current density during any stage test. We deter-
749 mined the operating voltage from a voltage vs. current
750 test performed at the lowest diluate conductivity (0.5
751 mS/cm), shown in Fig. A.1.

752 *Appendix A.3. Determination of diluate circuit volume*
753

754 We determined the diluate circuit volume by mea-
755 suring the change in salinity (via conductivity) of the

Symbol	Value	Ref.
<i>Membrane Performance Parameters</i>		
T_s	0.97	[42]
T_w	10	[42]
L_w	8.12×10^{-5} mol/bar-m ² -s	[42]
L_s	5.02×10^{-8} m/s	[42]
$\bar{r}_{am}, \bar{r}_{cm}$	$6.0 \Omega \text{ cm}^2$	[42]
σ	0.69	[31]
<i>Solution Properties</i>		
D	1.61×10^{-9} m ² /s	[33]
t_{cu}	0.5	[43]
<i>Flow Properties/Geometry</i>		
h	0.7 mm	-
A_m	271 cm ²	-
n_{cp}	17	-
V_{circ}	0.5367 L	-
Sh	20	[42]
<i>Operational Conditions</i>		
V	8 V	-
V_{el}	2 V	[42]

Table A.1: Key parameters used to model salt and water transport across membranes in the electro dialysis stack in order to determine steady-state concentrate salinities for each stage

diluate solution following the addition of a known amount of salt.

We initially filled the diluate beaker to the 1 L mark with deionised water. We then added a small, known mass of salt, w_s , to the beaker and turned the pumps on. We measured the steady-state conductivity to determine the concentration, C_d in mol/L, of the diluate circuit:

$$C_d = \frac{k_d}{\lambda_d} \quad (\text{A.2})$$

where k_d is the diluate conductivity in S/m and λ_d is the conductance in m²/Ω equiv. We then converted this concentration to molality, $m_{s,d}$, and solved for the

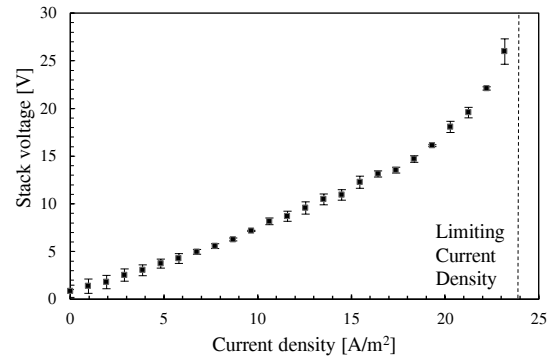


Figure A.1: Voltage vs current test with diluate and concentrate conductivities of 0.5 mS/cm.

volume of the circuit, V_{circ} :

$$V_{circ} = \frac{w_s}{M_s \rho_w m_{s,d}} \quad (\text{A.3})$$

758 where M_s is the molar mass of salt (kg/mol) and ρ_w
759 is the density of distilled water at 25°C. After repeat-
760 ing the measurement three times, we obtained a diluate
761 circuit volume of 0.54 ± 0.02 L.

762 Appendix B. Assessment of pumping power

763 We calculated the required pumping power by measur-
764 ing the pressure drop in the diluate circuit, ΔP , and
765 multiplying by the diluate flow rate, \dot{V} , held at 76 L/hr
766 for each stage. To compute the total pumping power,
767 we assumed the pressure drops in the diluate and con-
768 centrate circuits to be equal and multiplied by a factor
769 of two. We discounted the pumping power to drive the
770 rinse circuit since in a large scale system the number
771 of cell pairs per stack is large and hence the ratios of
772 diluate and concentrate flow rates to the rinse flow rate
773 would be small.

We made pressure measurements after flushing the
stack with distilled water and operating with diluate,
concentrate, and rinse feeds below 500 ppm. Thus we
neglected the effect of salinity on density and viscosity.
Multiplying by the specific process time of each stage,
 τ_i , we computed and plotted the specific pumping en-
ergy (See Figure 10):

$$E_{p,i}^w = 2 \dot{V} \Delta P \tau_i^w \quad (\text{B.1})$$

774 For the high salinity stages (numbers 5 and below),
775 the specific pumping energy makes up less than 5% of
776 the total specific energy consumed and the contribu-
777 tion to the total specific cost of energy is negligible.
778 In the low salinity stages, the specific pumping energy
779 makes up as much as 40% of the total specific energy
780 consumed. However, this number is largely a charac-
781 teristic of the small process length of the laboratory
782 scale system used. The relative contribution of stack
783 entrance and exit effects to pressure drop is large rel-
784 ative to frictional pressure drop through the passages
785 between the membranes.

786 Appendix C. Electrodialysis model

787 Appendix C.1. Concentration polarisation

The difference between bulk and membrane wall
concentrations and osmotic pressures is accounted for
by a convection-diffusion model of concentration pol-
arisation:

$$\Delta C = - \frac{(\bar{T}_{cu} - t_{cu}) i}{D} \frac{2h}{F \text{Sh}} \quad (\text{C.1})$$

where D is the solute diffusivity, F is Faraday's con-
stant, h is the channel height and t_{cu} is the counter-ion
transport number in the diluate and concentrate solu-
tions and is approximated as 0.5 for both anions and
cations. \bar{T}_{cu} is the integral counter-ion transport num-
ber in the membrane that accounts for both migration
and diffusion. It is assumed to be equal in the anion
and cation exchange membranes and approximated as:

$$\bar{T}_{cu} \approx \frac{T_s^{cp} + 1}{2}. \quad (\text{C.2})$$

For the a priori calculations of concentrate salinities
in Appendix A.1, the Sherwood number is computed
using the correlation obtained by Kuroda et al. [44] for
spacer A in their analysis:

$$\text{Sh} = 0.5 \text{Re}^{1/2} \text{Sc}^{1/3} \quad (\text{C.3})$$

where Sc is the Schmidt number, calculated using the
limiting diffusivity of NaCl in water [33] and the kine-
matic viscosity of pure water ν [45], both at 25°C. Re
is the Reynolds number defined as:

$$\text{Re} = \frac{2hV}{\nu} \quad (\text{C.4})$$

where V is the mass averaged velocity in the channel.

Appendix C.2. Junction and membrane potentials

Junction potentials associated with concentration
polarisation are neglected (which is compatible with
taking the transport number of both Na and Cl in solu-
tion as 0.5), while the sum of the anion and cation
membrane potentials $E_{am} + E_{cm}$ is computed consid-
ering quasi-equilibrium migration of salt and water
across the membranes:

$$E_{am} + E_{cm} = \frac{T_s^{cp}}{F} (\mu_{s,c,m} - \mu_{s,d,m}) + \frac{T_w^{cp}}{F} (\mu_{w,c,m} - \mu_{w,d,m}) \quad (\text{C.5})$$

where μ_s denotes the chemical potential of salt and μ_w
the chemical potential of water; both calculated em-
ploying osmotic coefficients and NaCl activity coeffi-
cient data from Robinson and Stokes [33]. The sub-
scripts c and d denote the concentrate and diluate while
the subscript m denotes a concentration at the mem-
brane surface.

Appendix D. Determination of fitted parameters

Appendix D.1. Sherwood number

The Sherwood number was determined via the lim-
iting current density. A current-voltage test was re-
peated three times for diluate and concentrate conduc-
tivities of 0.5 mS/cm, the results of which are shown in
Fig. A.1. The Sherwood number was then determined

by considering the following relationship between it and the limiting current density:

$$i_{lim} = \frac{D_{NaCl} F C_d S h}{2h \left(\frac{T_s + 1}{2} - t_{cu} \right)}. \quad (D.1)$$

799 with D_{NaCl} the diffusivity of sodium chloride in solu-
800 tion, F Faraday's constant, C_d the diluate concentra-
801 tion, h the concentrate and diluate channel heights and
802 T_s the salt transport number. The Sherwood number
803 was found to equal 18 ± 1 (68% confidence).

804 Appendix D.2. Spacer shadow factor

805 The spacer shadow factor, σ , quantifies the conduc-
806 tance of the diluate and concentrate channels relative
807 to what the conductance would be were there to be no
808 spacer. When the diluate and concentrate solutions are
809 of high conductivity the stack voltage is insensitive to
810 the spacer shadow factor, since the membrane resis-
811 tance dominates. Therefore, in determining σ we con-
812 sidered tests where the diluate and concentrate conduc-
813 tivities were low (0.5, 1.5, 2.5 and 7.5 mS/cm). We also
814 considered low values of current density (9.7, 19.3 and
815 29 A/m²) where the voltage-current relationship was
816 only weakly affected by concentration polarisation.

The stack voltage data was first corrected (from
 V_{stack} to V_{corr}) to remove the effects of concentra-
tion polarisation, employing the Sherwood number
from Appendix D.1 and the model described in Ap-
pendix C.1. This allowed the voltage current relation-
ship to be represented by:

$$V_{corr} = (2n_{cp} + 1)i\bar{r}_m + \frac{2Nih}{\sigma k} + \frac{2ih_r}{\sigma k_r} + V_{el} \quad (D.2)$$

where the terms on the right hand side represent volt-
age drops across the membranes, the diluate and con-
centrate (both at the same conductivity), the rinse
solutions and the electrodes, respectively. Plotting
 V_{corr} versus the inverse conductivity of the solution in
Fig. D.1 allowed σ to be determined from the slope.
Considering:

$$m = \frac{2Nih}{\sigma}, \quad (D.3)$$

817 where m is the slope of each of the lines in Fig. D.1, we
818 determined the spacer shadow effect at the three differ-
819 ent current densities. Since σ should be independent of
820 current density we computed its value as the average of
821 these three values, giving $\sigma = 0.64 \pm 0.03$.

822 Appendix D.3. Electrode potential

At low current densities the electrode potential was
computed considering the intercept c of each of the
lines in Fig. D.1:

$$V_{el} = c - (2N + 1)i\bar{r}_m + \frac{2ih_r}{\sigma k_r}. \quad (D.4)$$

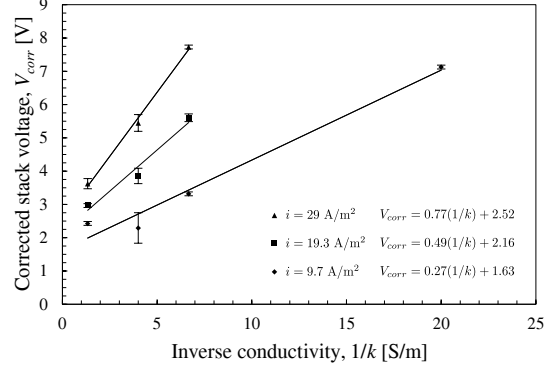


Figure D.1: Determination of spacer shadow effect and electrode potential at low voltage. The markers represent experimental values while the solid lines represent the fitted equations.

At low current densities, the determination of V_{el} is relatively insensitive to the voltage drop across the membranes and the rinse solutions since both are small. Therefore, even though \bar{r}_m is not known a priori, it is reasonable to assume $\bar{r}_m = 3 \times 10^{-4} \Omega \text{ m}^2$, in line with the membrane resistance quoted by the manufacturer [46]. The values of V_{el} found at 9.7, 19.3 and 29 A/m² were 2.4 ± 0.1 , 1.9 ± 0.3 and 2.2 ± 0.3 , respectively.

To determine the electrode potential at higher current densities, current-voltage tests were carried out with diluate and concentrate conductivities of 25 mS/cm, 75 mS/cm and 150 mS/cm (Fig. D.2). The linearity of these plots at high current densities (above approximately 240 A/m²) illustrates that neither membrane resistance nor electrode potential is a strong function of current density at high current densities. Furthermore, for these three conductivities, the range of current densities illustrated is far below the limiting current density and the voltage correction for concentration polarisation is thus negligible (*i.e.* $V_{stack} \approx V_{corr}$). The electrode potentials, calculated considering the intercept of the linear fits shown in Fig. D.2 (see Eq. D.2), for data taken at 25 mS/cm, 75 mS/cm and 150 mS/cm were found to be 1.5 ± 0.5 , 2.4 ± 0.25 and 2.3 ± 0.4 V, respectively. On the basis of electrode potentials thus being similar at low and high current density, a value of $V_{el} = 2.13 \pm 0.4$ V was considered for the model over the entire range of current densities.

Appendix D.4. Membrane resistance

At low diluate and concentrate conductivities the stack voltage is insensitive to the membrane resistance. Thus, we determined the membrane resistance from the high conductivity data of Fig. D.2. The membrane resistance at each value of conductivity was determined using the slope of a linear fit,

$$m = (2N + 1)\bar{r}_m + \frac{2Nh}{\sigma k} + \frac{2h_r}{\sigma k_r}, \quad (D.5)$$

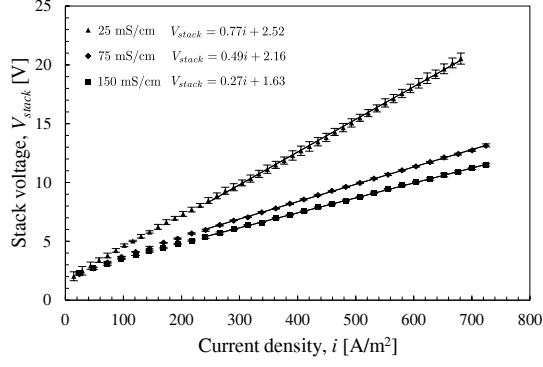


Figure D.2: Determination of membrane resistances and electrode potentials from high conductivity data. The markers represent experimental values while the solid lines represent the fitted equations.

knowing already the value of σ from Appendix D.2. The values of membrane resistance found for solution conductivities of 25 mS/cm, 75 mS/cm and 150 mS/cm were $4.5 \times 10^{-4} \pm 5 \times 10^{-5}$, $2.8 \times 10^{-4} \pm 3 \times 10^{-5}$ and $3.0 \times 10^{-4} \pm 5 \times 10^{-5} \Omega \text{ m}^2$. Thus, the membrane resistance was modelled as $3.5 \times 10^{-4} \pm 1 \times 10^{-4} \Omega \text{ m}^2$ over the entire range of diluate and concentrate salinities.

Appendix D.5. Salt and water transport numbers

Salt and water transport numbers at solution conductivities of 7.5 mS/cm, 75 mS/cm, 150 mS/cm and 225 mS/cm were determined by running tests at constant current and measuring the mass of salt and water transported across the membranes in a fixed amount of time. Three tests were performed at each set of conditions to ensure repeatability. During these tests, an approximately constant concentrate conductivity was maintained by selecting an initial concentrate solution volume that was three times that of the diluate. The concentrate beaker was filled with NaCl solution of the desired conductivity and the diluate beaker was filled with NaCl solution that was 1.5, 5, 15 and 15 mS/cm higher than the concentrate conductivity for the 7.5, 25, 75 and 150 mS/cm cases, respectively. The pumps were turned on and a constant current was applied across the stack. The diluate mass and conductivity were recorded until the diluate conductivity reached a value 1.5, 5, 15 and 15 mS/cm below that of the concentrate for the 7.5, 25, 75 and 150 mS/cm cases, respectively. The salt and mass transport numbers were then determined by Eq. (D.6) and Eq. (D.7):

$$T_s^{cp} = \frac{\Delta w_{s,d} F}{n_{cp} I \Delta t M_s} \quad (\text{D.6})$$

$$T_w^{cp} = \frac{\Delta w_{w,d} F}{n_{cp} I \Delta t M_w T_s}. \quad (\text{D.7})$$

Here, $\Delta w_{s,d}$ and $\Delta w_{w,d}$ were the changes in the diluate mass for salt and water respectively, F Faraday's constant, I the applied current across the membrane

(10 A), N_{cp} the number of cell pairs, and Δt the process run time. The temperature was held constant at 25°C and the diluate mass was corrected for leakage from diluate to concentrate (determined through leakage tests performed at zero current with deionised water in the concentrate and diluate chambers). Bias errors arising from determining the diluate circuit volume (Appendix A.3) and leakage were propagated through Eqs. (D.7) and (D.6) and combined with the random error [Eq. (12)] that was determined from the sample standard deviation of results from the three tests run at the same conditions. As shown in figure D.3, the salt transport numbers are decreasing with increasing conductivities due to the falling charge density of membranes relative to the solutions [47]. Figure D.4 shows that the water transport numbers are also decreasing with increasing conductivities because of falling water activity, which reduces the membranes' capacity to hydrate [48].

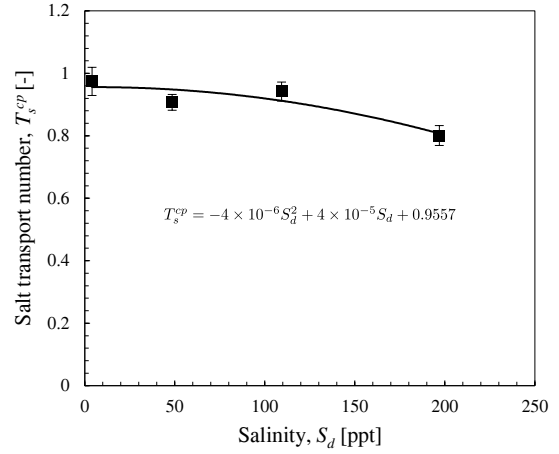


Figure D.3: Salt transport number. The markers represent experimental values while the solid lines represent the fitted equations

Appendix D.6. Salt and water permeability

The permeabilities of the membranes to salt and water at solution conductivities of 7.5 mS/cm, 75 mS/cm, 150 mS/cm and 225 mS/cm were determined by running tests at zero current with de-ionised water flowing in the diluate compartment. Three tests were performed at each value of concentrate conductivity to ensure repeatability. During these tests, an approximately constant concentrate conductivity was maintained by selecting an initial concentrate solution volume that was three times that of the diluate. The pumps were turned on and data for diluate conductivity and mass were recorded versus time. Throughout the tests, the temperature was held constant at 25°C. The tests were stopped after the diluate concentration reached conductivities of 200 $\mu\text{S/cm}$, 900 $\mu\text{S/cm}$, 900 $\mu\text{S/cm}$ and

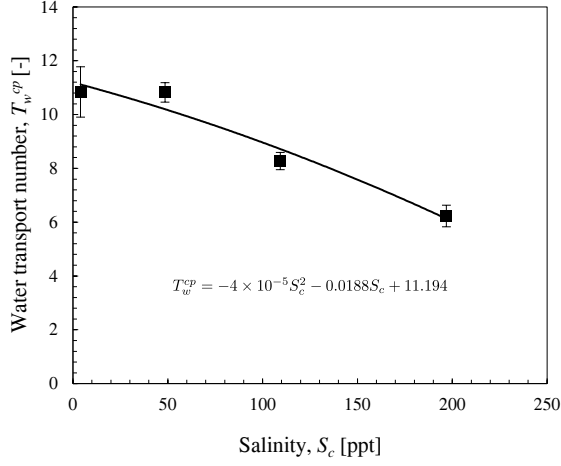


Figure D.4: Water transport number. The markers represent experimental values while the solid lines represent the fitted equations

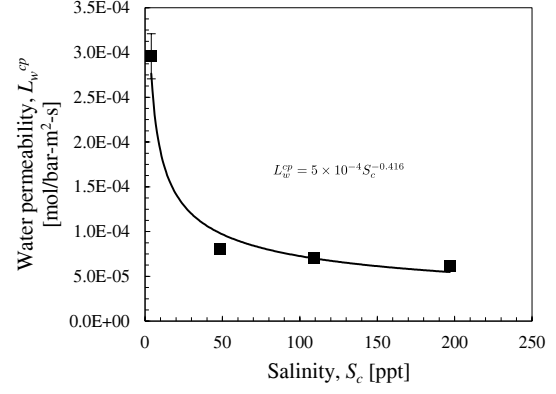


Figure D.6: Water permeability. The markers represent experimental values while the solid lines represent the fitted equations

3,200 $\mu\text{S}/\text{cm}$ for the four values of concentrate conductivity respectively. The salt and water permeability coefficients were determined employing Eqns. (D.8) and (D.9)

$$L_s^{cp} = \frac{J_s}{(C_c - \frac{\Delta C_d}{2}) A_m N_{cp}} \quad (\text{D.8})$$

$$L_w^{cp} = \frac{J_w}{\Delta \pi A_m N_{cp}} \quad (\text{D.9})$$

with A_m the active membrane area and N_{cp} the number of cell pairs in the stack. A second order polynomial fit was applied to the salt permeabilities and a power-law fit was applied to the water permeabilities. Bias errors arising from determining the diluate circuit volume (Appendix A.3) and leakage were propagated through Eqs. (D.7) and (D.6) and combined with the random error [Eq. (12)] arising from the sample standard deviation of results from the three tests run at the same conditions.

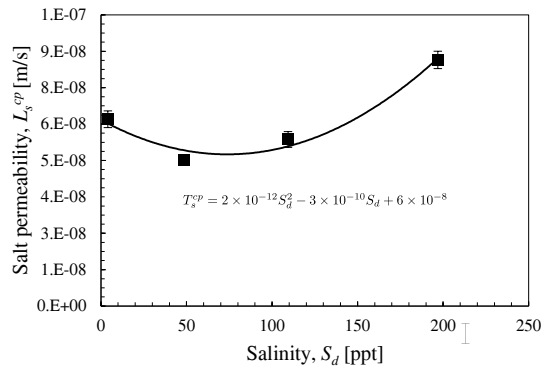


Figure D.5: Salt permeability. The markers represent experimental values while the solid lines represent the fitted equations

Appendix D.7. Summary of model parameters

A summary of the model parameters and equations is provided in Table D.2. Membrane salt transport, water transport, salt permeability and water permeability are modelled as:

$$T_s^{cp} = -4 \times 10^{-6} S_d^2 + 4 \times 10^{-5} S_d + 0.96 \pm 0.04 \quad (\text{D.10})$$

$$T_w^{cp} = -4 \times 10^{-5} S_c^2 - 1.9 \times 10^{-2} S_c + 11.2 \pm 0.6 \quad (\text{D.11})$$

$$L_s^{cp} = \min(2 \times 10^{-12} S_d^2 - 3 \times 10^{-10} S_d + 6 \times 10^{-8}, 2 \times 10^{-12} S_c^2 - 3 \times 10^{-10} S_c + 6 \times 10^{-8}) \pm 6 \times 10^{-9} [\text{m/s}] \quad (\text{D.12})$$

$$L_w^{cp} = 5 S_c^{-0.416} \pm 2 \times 10^{-5} [\text{mol}/\text{m}^2 \text{s bar}] \quad (\text{D.13})$$

Symbol	Value	Ref.
<i>Solution Properties</i>		
D	$1.61 \times 10^{-9} \text{ m}^2/\text{s}$	[33]
t_{cu}	0.5	[43]
ν	$8.9 \times 10^{-7} \text{ m}^2/\text{s}$	[45]
<i>Flow Properties/Geometry</i>		
h	0.5 mm	-
n_{cp}	17	-
Sh	18	-
<i>Membrane Parameters</i>		
σ	0.64 ± 0.03	-
\bar{r}_m	$3.5 \times 10^{-4} \pm 1 \times 10^{-4} \text{ } \Omega \text{ m}^2$	-
T_s^{cp}	Eq. (D.10)	-
T_w^{cp}	Eq. (D.11)	-
L_s^{cp}	Eq. (D.12)	-
L_w^{cp}	Eq. (D.13)	-
<i>Stack Parameters</i>		
V^{cp}	8 V	-
V_{el}	$2.1 \pm 0.4 \text{ V}$	-

Table D.2: Electrodialysis Model Parameters